Plasmonics (2022) 17:2031–2036
https://doi.org/10.1007/s11468-022-01690-z

Tunable Perfect Absorber from Visible to Near-infrared with Insensitive Properties to Incident Angle and Polarization

Yuanhang Zhao[1,2] · Yuchen Lin[1,2] · Ying Xiong[1,2] · Zizheng Li[3] · Xiaoyi Wang[1] · Jinsong Gao[1,2]

Received: 19 May 2022 / Accepted: 2 July 2022 / Published online: 3 August 2022

Abstract

In this paper, we propose an Insulator-Metal-Insulator-Metal (IMIM) nano-block array structure, which can achieve tunable single-peak and double-peak perfect absorption properties from visible light to near-infrared. Compared with our previous work, this paper additionally points out that due to the coupling effect between SPPs, the original blue-shifted spectrum is converted into red-shifted during the process of changing the thickness ratio of the middle silver nano-block to the SiO2 nano-block. In the design parameter range, two different structural parameters can be found, in which the absorption peak is exactly the same, and the short-wave absorption peak position has the characteristics of "on" and "off". Based on the nature of absorption spectrum, it can be applied to optical switches in optical circuits. And this work also provides a new idea for plasma sensors, which has broad application prospects in the fields of filtering and imaging.

Keywords Insulator-Metal-Insulator-Metal · Surface plasmon polariton · Gap-plasmon guided mode · Optical switches

Introduction

Realizing the interaction between light and matter using metasurface structure is one of the hottest topics nowadays [1, 2]. The emergence of surface plasmons breaks the limitation of diffraction. From the form of expression, surface plasmons (SPs) are mainly divided into surface plasmons propagating (SPP) at the metal-dielectric interface and localized surface plasmons (LSP) confined around the nanostructure geometry [3–5]. By designing the shape, size, and material of the metasurface structure, the optical properties such as phase, amplitude, polarization, and coherence can be modulated [6]. It provides a feasible solution for researchers to manipulate the electromagnetic response. The unique and remarkable maneuverability of the plasma metasurface structure on light makes that plasmonic devices have broad application prospects, such as biochemical sensors [7–9], energy harvesting [10–13], nonlinear optics [14, 15], photocatalysts [6, 16], and surface enhanced Raman scattering (SERS) [17–19].

Plasma perfect absorbers [20, 21] have important application potential in the fields of thermal radiation [22], photodetectors [23, 24] and sensing [25, 26]. In recent years, the plasma perfect absorber has been studied deeply from

Yuchen Lim, Ying Xiong, Zizheng Li, Xiaoyi Wang, and Jinsong Gao contributed equally to this work.

✉ Zizheng Li
lizizheng87@163.com

Yuanhang Zhao
Zhaoyhciomp@163.com

Yuchen Lin
945700739@qq.com

Ying Xiong
xiongying18@mails.ucas.ac.cn

Xiaoyi Wang
wangxiaoyi1977@sina.com

Jinsong Gao
gaojs999@163.com

[1] Key Laboratory of Optical System Advanced Manufacturing Technology, Changchun Institute of Optics, Fine Mechanics and Physics, Chinese Academy of Sciences, Southeast Lake Road, Changchun 130033, Jilin, China

[2] College of Materials Science and Opto-Electronic Technology, University of the Chinese Academy of Sciences, Yanqi Lake Campus, Beijing 100039, Beijing, China

[3] MOE Key Laboratory of TianQin Mission, TianQin Research Center for Gravitational Physics and School of Physics and Astronomy, Frontiers Science Center for TianQin, Gravitational Wave Research Center of CNSA, Sun Yat-sen University, Zhuhai Campus, Zhuhai 519082, Guangzhou, China

both theory and experiment. The shape, size, and material of the metasurface structure have an effective modulation effect on the spectrum [6]. Therefore, lots of metasurface structures with excellent results have appeared, such as metal gratings [27, 28], nanohole arrays [29], nano-block arrays [30–32], and nano-cone [33] structures. Insulator-metal (IM) is a common structural unit of plasma absorbers. Using this basic structure, plasma super-absorbers exhibit spectral tunability and can achieve almost perfect absorption characteristics [34, 35].

In this paper, we adopt the IMIM four-layer structure. By designing and optimizing the structural parameters, its reflection was suppressed at the resonance wavelength, and the near-perfect absorption from the visible light to the near-infrared is achieved. Figure 1 is a schematic diagram of the IMIM structure of the tunable perfect absorber. When selecting materials, we consider that silver has the characteristics of high reflection and low absorption, and has excellent optical properties in the range of visible light to near-infrared. SiO2 is the most used low refractive index dielectric material with high stability and mature preparation technology. We constructed a SiO2-Ag-SiO2 nano-block structure with periodic boundary conditions on glass substrate coated with 200-nm-thick Ag layer. By adjusting the size of the nanostructures, single-peak and double-peak two kinds of absorption properties from visible light to near-infrared can be achieved, that is, the appearance of short-wave resonance peaks can be regulated under the condition that the long-wave resonance peaks are exactly coincident.

Simulation Modeling

In order to effectively analyze the final response of the plane wave perpendicular to the superabsorbent, we use the commercial software Lumerical FDTD Solutions to simulate the IMIM structure. The incident light source is set to TM linear polarized light with a resonant electric field polarized along the X axis, which illuminates the system surface perpendicularly. Set the X and Y axes in the simulation area as periodic boundary conditions. In order to eliminate echo interference, the Z axis is set to a perfect matching layer (PML). To ensure the convergence of the simulation structure, we use a higher mesh accuracy (mesh=2 nm). The definition of structure size caters to the needs of optical devices to be miniaturized and lightweight. The total height H, period P, and side length D of the nano-block are 128 nm, 420 nm, and 84 nm, respectively. The thickness of Ag in the middle of the nano-block is T=Zmax−Zmin, and the fixed Zmax=108 nm. Finally, sweep the lower surface of the middle Ag nano-block Zmin, and the range of Zmin is 0–108 nm.

Results and Discussion

The simulated absorption is plotted as a function of Zmin and incident wavelength, as shown in Fig. 2. When the thickness of the underlying Ag layer is thick enough, the transmitted light will be completely suppressed, which is commonly more than 120 nm. As a result, the spectral intensity is equal to the sum of the absorption intensity and the reflection intensity (1=R+A). There are two absorption modes in Fig. 2, here we define them as mode A and mode B. For mode A, with the decrease of the thickness ratio of Ag nano-blocks and SiO2 nano-blocks in the middle layer, the resonance wavelength position hardly changes, but the corresponding mode intensity will be significantly reduced, and finally disappear completely. For mode B, as the thickness ratio of the Ag nano-blocks and the SiO2 nano-blocks in the middle layer decreases, the resonance wavelength position firstly trends to blue shift and then red shift. When the height Zmin of the bottom surface of the Ag nano-block

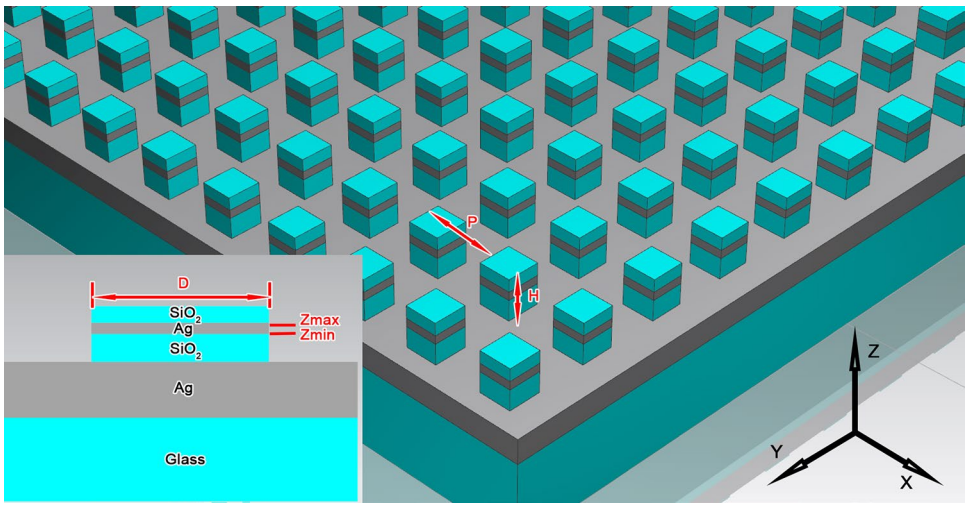

Fig. 1 IMIM plasma perfect absorber structure diagram, SiO2-Ag-SiO2 nano-block structure on glass substrate coated with 200-nm-thick Ag layer

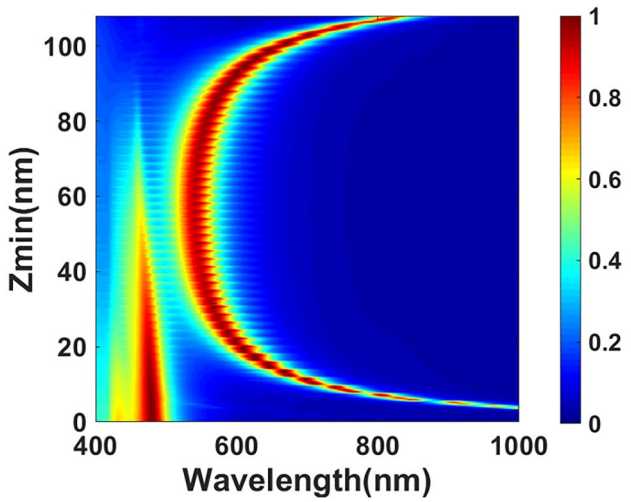

Fig. 2 Scanning reference map for Zmin height of the bottom surface of Ag nano-block (0 nm<Zmin<108 nm)

increases to around 60 nm, the mode A almost disappears, and at the same time, the mode B has a blue shift trend. We can find the resonance position with the peak intensity nearly the same within the 550–1000 nm band, and at the same time can artificially control the appearance of the resonance peak at 480 nm.

When setting two characteristic thicknesses of middle Ag layer in nano-blocks (T=14.5 nm, 93 nm), the resonance peaks at the wavelength of 644 nm exhibit almost the same absorption, and their intensities are both as high as 99.9%, as shown in Fig. 3. While the absorption peak near the wavelength of 480 nm only appears when the thickness of the middle Ag layer in the nano-block is equal to 93 nm, and

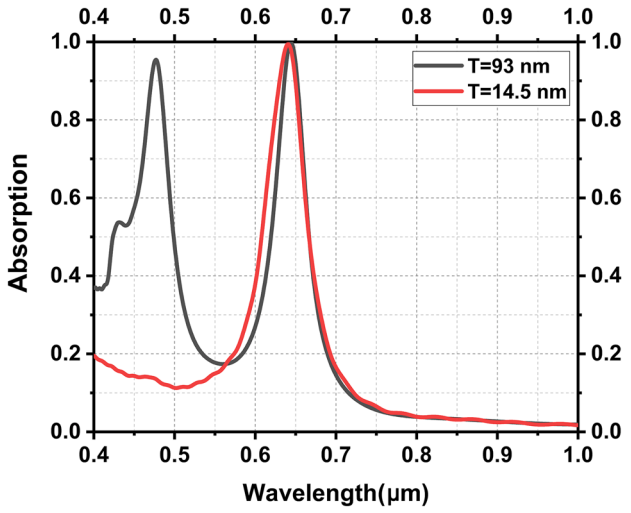

Fig. 3 Absorption spectra of different thick middle Ag layer in the nano-block (T=14.5 nm and 93 nm)

the peak intensity is close to 95%. Therefore, when reducing the thickness of the middle Ag layer in the nano-block, the mode A is greatly suppressed, and the peak intensity of the mode B is little affected. By adjusting the thickness of the middle Ag layer, the single-peak and double-peak can be controlled in the visible and near-infrared range, and the average absorption is more than 99%.

Each thickness of middle Ag layer in the nano-block can find a corresponding different value within the thickness variation range that the peak intensity and resonance wavelength position of these two situations are almost the same. Therefore, it can be realized that when keeping the absorption characteristics at 644 nm constant, the appearance of the absorption peak at 477 nm can be controlled. This excellent optical characteristic can be used to optical switches in optical computing [36]. The modes A and B in the absorption spectrum correspond to two optical signals A (absorption peak at 477 nm wavelength) and B (absorption peak in the long-wavelength range). The appearance and disappearance of the two light signals respectively represent the logic "1" and the logic "0" in the logic gate. The absorption peak of mode B always exists which is in the logic "1" state, so the switching performance can be achieved through mode A. If an "AND" gate is placed in front of the two optical signals, the optical signals (1,1) and (0,1) represent the two states of "on" and "off" respectively. As shown in Fig. 2, this structure can be applied in the visible light to near-infrared waveband, which enhances its application potential.

In order to explore the physical mechanism of each absorption peak, we deeply studied on each absorption mode. Localized surface plasmons (LSPRs) are more sensitive to the size, shape, and materials of nanostructures, while surface plasmons (SPPs) are more sensitive to changes in structure period and incident angle of light. For mode A, as the thickness of middle Ag layer in the nano-block increases, there is almost no change in the resonance wavelength position. The following dispersion relation can be used to describe this behavior [37]:

$$\lambda_{spp} = \frac{P}{\sqrt{i^2 + j^2}} \sqrt{\frac{\epsilon_m \epsilon_d}{\epsilon_m + \epsilon_d}} \tag{1}$$

where ϵ_m, ϵ_d represent the dielectric constant of the metal in the system and the dielectric constant of the insulator, λ_{spp} corresponds to the wavelength of the absorption peak, P=480 nm is the structure period, and i, j are resonance orders. When $\lambda = \lambda_{spp}$, the energy carried by the incident electromagnetic wave will propagate outward along the interface between the metal and the insulator. The wavelength of the absorption peak corresponding to mode A λ_{spp} is 477 nm, and the result calculated by the above formula is 510 nm, and the deviation is about 30 nm. The FDTD simulation software is used to analyze the electric field

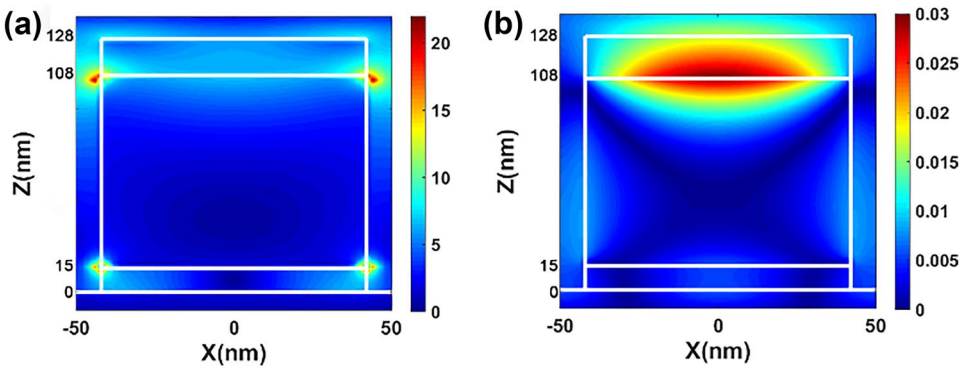

Fig. 4 **a** and **b** Distribution diagram of electric and magnetic field at absorption peak = 480 nm

and magnetic field distribution at the absorption peak λ_{spp} =477 nm, as shown in Fig. 4. It can be seen that the composition of mode A is not only the SPP mode at the SiO2/Ag interface, but also weaker mode resonances are also excited at the lower interface of the Ag nano-block and on both sides. Under the premise that the SPP mode at the upper SiO2/Ag interface plays a dominant role, the peak position is deviated from the calculated result due to the weak mode resonance excited by the nanostructure.

For mode B, the electric and magnetic field distributions at the resonance wavelength of 644 nm are shown in Fig. 5. In Fig. 5(a) and (b), the electric and magnetic field energy is confined between the nano-block Ag layer and the underlying Ag layer, and the resonance peak is caused by the gap plasma mode. The resonance wavelength is reflected back and forth between the upper and lower Ag layers, to create cavity resonance [38]. This gap plasma mode is not sensitive to the angle and polarization of the incident light. In Fig. 5(c) and (d), the electric and magnetic field energy is confined to the upper and lower interfaces of nano-blocks, which are mainly generated by the SPP mode at the SiO2/Ag interface and Ag/SiO2 interface. The decrease in the thickness ratio of Ag to SiO2 nano-block layers leads to weaker interaction between Ag nano-blocks and silver film. As the thickness of the SiO2 nano-block increases, the SPP mode at the Ag/SiO2 interface will dominate [39]. For the IMI structure, when the thickness of the middle Ag layer of nano-block is gradually reduced to the penetration depth of the incident light, the SPP modes generated at the upper and lower interfaces will be coupled, and a stronger new mode will finally be generated [40]. By analyzing the penetration depth of the incident light $L = |(\epsilon_m + \epsilon_d) \div (\epsilon_m \epsilon_d)| \, 0.5/k_0$, we can

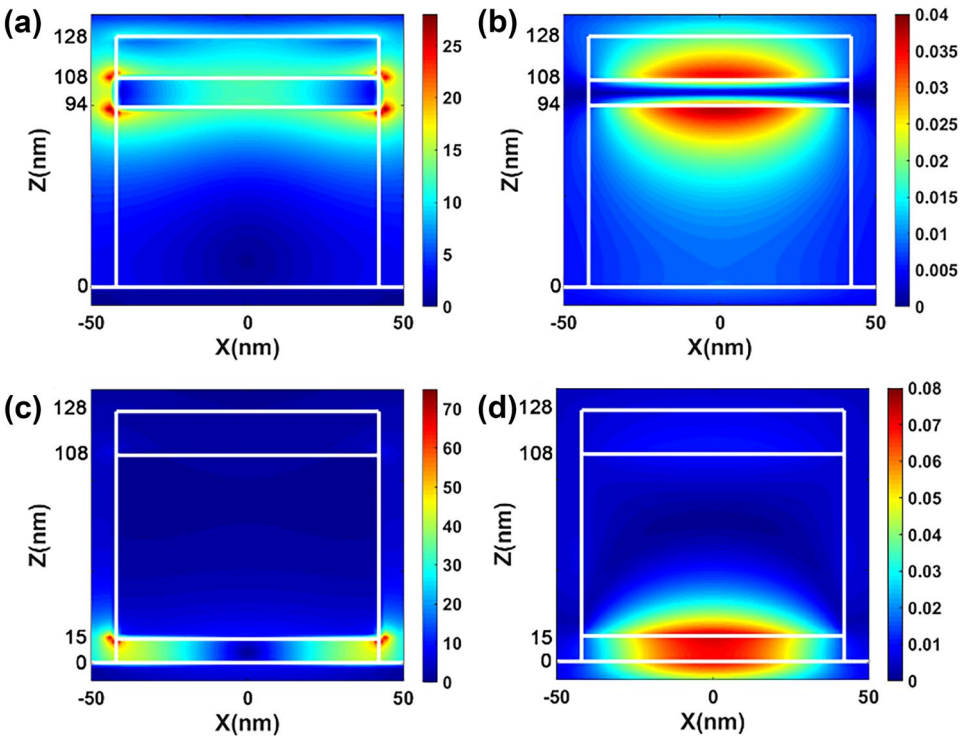

Fig. 5 **a** and **b** Electric and magnetic field distribution diagram of the double absorption peak curve at = 641 nm; **c** and **d** Electric field and magnetic field distribution diagram of the single absorption peak curve = 641 nm

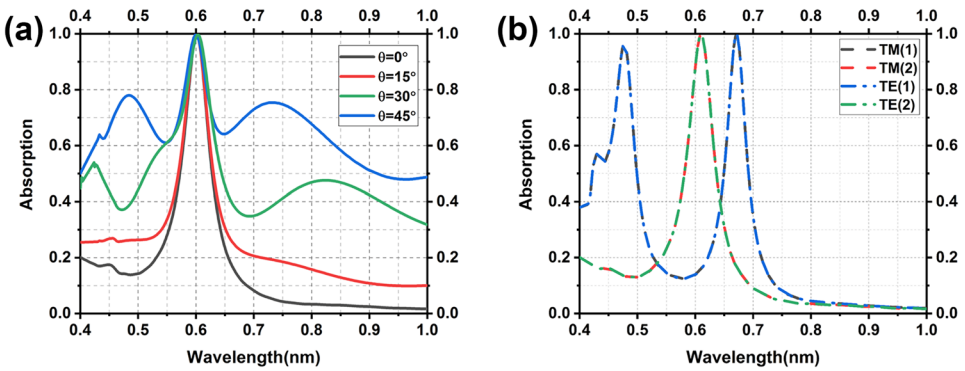

Fig. 6 Absorption spectrum curves at incident angles of 0°, 15°, 30° and 45°; **b** Comparison of absorption spectrum curves under TE and TM polarization states

calculate the range of the penetration depth L of the incident light penetrating the Ag nano-block (23 nm<L<25 nm). When the thickness T (T=Zmax − Zmin≤L, the SPP modes of the upper and lower interfaces are coupled. Zmax is a fixed value of 108 nm. When Zmin>83 nm, mode A will disappear from the spectral curve. This result is confirmed in Fig. 2. Mode A disappears completely near Zmin equal to 83 nm.

The sensitivity of the incident angle is often one of the main factors which affect the optical performance. Some related optical systems need to maintain specific optical characteristics at a large incident angle. Breaking the limitation of the angle can make the application scenarios of the structure wider. Based on this, different absorption curves at the incident angles of 0°, 15°, 30°, and 45° are as shown in Fig. 6(a). With the incident angle increasing, the absorption intensity at 600 nm still maintains nearly perfect absorption, and the overall absorption rate will increase significantly. The perfect absorption of a specific wavelength can still be achieved at the incident angle of 45°. For the polarization of the incident light, we have carried out multiple comparisons, such as Fig. 6(b). Comparing the absorption spectrum curves of TM and TE waves at the two nano-block thicknesses, they maintain a high degree of consistency. It is proved that this structure is not sensitive to the polarization of incident light and can be used for depolarization optical systems. The insensitivity of the incident angle and the polarization state of the incident light broadens application range.

Conclusion

In summary, we have investigated a single-peak and double-peak tunable plasma filter based on the IMIM structure in the visible light to near-infrared (0.4–1 μm). By adjusting the thickness ratio of the SiO2 layer and the Ag layer in the nano-block, flexible control can be achieved while ensuring the perfect absorption of single-peak mode and double-peak mode. Through the SPP mode, the coupling between SPP modes, and the gap plasma mode, the physical mechanism of absorption at each position is revealed. Finally, it is confirmed that the structure is insensitive to the angle and polarization of the incident light. In addition, combined with the excellent characteristics of absorption spectrum, the application in optical switches is proposed, which broadens its application range. At the same time, the advantages of structure thickness ratio modulation and size miniaturization are suitable for integration with photonic devices.

Author Contribution Li Zizheng and Zhao Yuanhang explored the conception and design of the article. Lin Yuchen and Xiong Ying modified the pictures in the article. Wang XiaoYi and Gao Jinsong made final revisions to the article.

Funding This project was supported by the National Natural Science Foundation of China (No. 61705226).

Availability of Data and Materials All data included in this article are available from the corresponding author upon reasonable request.

Code Availability All codes included in this article are available from the corresponding author upon reasonable request.

Declarations

Ethics Approval Not applicable

Consent to Participate Not applicable

Consent for Publication Not applicable

Competing Interests The authors declare no competing interests.

References

1. Neshev D, Aharonovich I (2018) Optical metasurfaces: new generation building blocks for multi-functional optics. Light Sci Appl 7:58
2. Malkiel I, Mrejen M, Nagler A, Arieli U, Wolf L, Suchowski H (2018) Plasmonic nanostructure design and characterization via Deep Learning. Light Sci Appl 7:60

3. Anatoly Z, Igor S (2003) Near-field photonics: Surface plasmon polaritons and localized surface plasmons. J Opt A: Pure Appl Opt 5:S16
4. Chu Y, Banaee MG, Crozier KB (2010) Double-resonance plasmon substrates for surface-enhanced raman scattering with enhancement at excitation and stokes frequencies. ACS Nano 4:2804
5. Chu Y, Crozier KB (2009) Experimental study of the interaction between localized and propagating surface plasmons. Opt Lett 34:244
6. Ma X-C, Dai Y, Yu L, Huang B-B (2016) Energy transfer in plasmonic photocatalytic composites. Light Sci Appl 5:e16017
7. Cetin AE, Etezadi D, Galarreta BC, Busson MP, Eksioglu Y, Altug H (2015) Plasmonic Nanohole Arrays on Robust Hybrid Substrate for Highly Sensitive Label-Free Biosensing. ACS Photonics 2:1167
8. Park B, Yun SH, Cho CY, Kim YC, Shin JC, Jeon HG, Huh YH, Hwang I, Baik KY, Lee YI, Uhm HS, Cho GS, Choi EH (2014) Surface plasmon excitation in semitransparent inverted polymer photovoltaic devices and their applications as label-free optical sensors. Light Sci Appl 30:e222
9. Cattoni A, Ghenuche P, Haghiri-Gosnet AM, Decanini D, Chen J, Pelouard J, Collin S (2011) 3/1000 Plasmonic Nanocavities for Biosensing Fabricated by Soft UV Nanoimprint Lithography. Nano Lett 11:3557
10. Watts CM, Liu XL, Padilla WJ (2012) Metamaterial electromagnetic wave absorbers. Adv Mater 24:98
11. Qu Y, Li Q, Gong H, Du K, Bai S, Zhao D, Ye H, Qiu M (2016) Spatially and Spectrally Resolved Narrowband Optical Absorber Based on 2D Grating Nanostructures on Metallic Films. Adv Optical Mater 4:480
12. Cao T, Wei C, Simpson RE, Zhang L, Cryan MJ (2015) Broadband Polarization-Independent Perfect Absorber Using a Phase-Change Metamaterial at Visible Frequencies. Sci Rep 4:3955
13. Liu K, Zeng X, Jiang S, Ji D, Song H, Zhang N, Gan Q (2014) A large-scale lithography-free metasurface with spectrally tunable super absorption. Nanoscale 6:5599
14. Klein MW, Wegener M, Feth N, Linden S (2008) Experiments on second- and third-harmonic generation from magnetic metamaterials. Opt Express 15:5238
15. Pala RA, White J, Barnard E, Liu J, Brongersma ML (2009) Design of Plasmonic Thin-Film Solar Cells with Broadband Absorption Enhancements. Adv Mater 21:3504
16. Khan ME, Cho MH (2019) Surface plasmon-based nanomaterials as photocatalyst. In book: Progress in Botany 80:173
17. Kahraman M, Ozbay A, Yuksel H, Solmaz R, Demir B, Caglayan H (2018) Tunable plasmonic silver nanodomes for surface-enhanced raman scattering. Plasmonics 13:785
18. Zheng P, Li M, Jurevic R, Cushing SK, Liu Y, Wu N (2015) A gold nanohole array-based surface-enhanced Raman scattering biosensor for detection of silver(i) and mercury(ii) in human saliva. Nanoscale 7:11005
19. Zheng P, Cushing SK, Suri S, Wu N (2015) Tailoring plasmonic properties of gold nanohole arrays for surface-enhanced Raman scattering. Phys Chem Chem Phys 17:21211
20. Jia XL, Meng QX, Yuan CX, Zhou ZX, Wang XO (2016) Visible light broadband perfect absorbers. Phys Plasmas 23:032103
21. She XY, Shen Y, Wang JF, Jin CJ (2019) Pd films on soft substrates: a visual, high-contrast and low-cost optical hydrogen sensor. Light Sci Appl 8:1
22. Xuan Y (2014) An overview of micro/nanoscaled thermal radiation and its applications. Photonics Nanostruct Fundam Appl 12:93
23. Chalabi H, Schoen D, Brongersma ML (2014) Hot-electron photodetection with a plasmonic nanostripe antenna. Nano Lett 14:1374
24. Abutoama M, Isaacs S, Ney M, Zhong L, Li D, Jiang L, Abdulhalim I (2019) Ultrahigh field enhancement optimization versus rabi splitting investigated using Au nano-bipyramids on metal film. J Phys Chem C 123:12984
25. Wu D, Li R, Liu Y, Yu ZY, Yu L, Chen L, Liu C, Ma R, Ye H (2017) Ultra-narrow band perfect absorber and its application as plasmonic sensor in the visible region. Nanoscale Res Lett 12:427
26. Talghader J, Gawarikar A, Shea R (2012) Spectral selectivity in infrared thermal detection. Light Sci Appl 1:e24
27. Zhou WC, Li KW, Song C, Hao P, Chi MB, Yu MX, Wu YH (2015) Polarization-independent and omnidirectional nearly perfect absorber with ultra-thin 2D subwavelength metal grating in the visible region. Opt Express 23:A413
28. Li SR, Yang HN, Shi HY, Jiang XQ, Sun XD (2020) Perfect absorption in symmetrical single layer ultrathin metal grating with unilateral illumination. Results Phys 18:2211
29. Tong H, Xu YQ, Su YW, Wang XX (2019) Theoretical study for fabricating elliptical subwavelength nanohole arrays by higher-order waveguide-mode interference. Results Phys 14:2211
30. Zhao YH, Li ZZ, Li Q, Wang K, Gao JB, Wang K, Yang HG, Wang XY, Wang TT, Wang YC, Gao JS (2021) Tunable perfect absorption structures based on cavity coupling and plasmon hybrid mode. IEEE Photonics J 13:1
31. Qian H, Li S, Chen C-F, Hsu S-W, Bopp SE, Ma Q, Tao AR, Liu Z (2019) Large optical nonlinearity enabled by coupled metallic quantum wells. Light Sci Appl 8
32. Hao J, Wang J, Liu X, Padilla WJ, Zhou L, Qiu M (2010) High performance optical absorber based on a plasmonic metamaterial. Appl Phys Lett 96:251104
33. Wang ZL, Duan GH, Duan HG (2021) Optimization of the perfect absorber for solar energy harvesting based on the cone-like nanostructures. AIMS Energy 9:714
34. Hubarevich A, Marus M, Fan WJ, Smirnov A, Wang H (2018) Highly efficient ultrathin plasmonic insulator-metal-insulator-metal solar cell. Plasmonics 13:141
35. Hubarevich A, Kukhta A, Demir HV, Sun XW, Wang H (2015) Ultra-thin broadband nanostructured insulator-metal-insulator-metal plasmonic light absorber. Opt Express 23:9753
36. Koch U, Hoessbacher C, Emboras A, Leuthold J (2017) Optical memristive switche. J Electroceram 39:239
37. Barnes WL, Dereux A, Ebbesen TW (2003) Surface Plasmon subwavelength optics. Nature 424:824
38. Moreau A, Ciraci C, Mock JJ, Hill RT, Wang Q, Wiley BJ, Chilkoti A, Smith DR (2012) Controlled-reflectance surfaces with film-coupled colloidal nanoantennas. Nature 492:86
39. Li YL, An B, Jiang SM, Gao J, Chen YL, Pan SD (2015) Plasmonic induced triple-band absorber for sensor application. Opt Express 23:17607
40. Maier SA (2007) Plasmonics: Fundamentals and Applications, Springer Chap. 2.3